Available online at www.sciencedirect.com

SciVerse ScienceDirect

Ceramics International 38 (2012) 3875–3883

CERAMICS INTERNATIONAL

www.elsevier.com/locate/ceramint

The role of substrate temperature on the properties of nanocrystalline Mo doped ZnO thin films by spray pyrolysis

R. Swapna, M.C. Santhosh Kumar *

Advanced Materials Laboratory, Department of Physics, National Institute of Technology, Tiruchirappalli 620 015, India

Received 25 November 2011; received in revised form 15 January 2012; accepted 15 January 2012
Available online 25 January 2012

Abstract

Transparent conducting molybdenum (2 at.%) doped zinc oxide (MZO) films were prepared with various substrate temperatures by spray pyrolysis technique on glass substrates. The effect of substrate temperature on the structural, surface morphological, electrical, optical and photoluminescence properties of these films were studied. The X-ray diffraction analysis revealed that the films are polycrystalline in nature having a wurtzite structure with a preferred grain orientation in the (0 0 2) direction. The average crystallite size of the films increases from 17 nm to 28 nm with the increase of substrate temperature from 573 K to 623 K, thereafter it slightly decreases with further increase of substrate temperature to 723 K. Analysis of structural parameters indicates minimum strain and stress values for films deposited at a substrate temperature of 673 K. From atomic force microscopy (AFM) analysis, it is found that rms roughness of the films deposited at 623 K is a minimum, indicating better optical quality. The scanning electron microscopy (SEM) measurements showed that the surface morphology of the films changes with substrate temperature. Optical parameters such as optical transmittance, reflectance, refractive index, extinction coefficient, dielectric constant and optical band gap have been studied and discussed with respect to substrate temperature. Room temperature photoluminescence (PL) spectra show the deep-level emission in the MZO thin films. The films exhibit a low electrical resistivity of 6.22×10^{-2} Ω cm with an optical transmittance of 75% in the visible region at a substrate temperature of 623 K.

Keywords: A. Films; B. Grain size; C. Optical properties; C. Electrical conductivity; D. ZnO

1. Introduction

Transparent conducting zinc oxide films have been extensively studied in recent years, because of their low cost precursor materials, relatively low deposition temperature and high stability in hydrogen plasma compared to ITO and SnO_2 films [1]. These advantages are of considerable interest for solar energy conversion appilications. ZnO have high chemical and thermal stability and high abundance make it an attractive material for a wide variety of applications, such as UV emitters and detectors, gas sensors, light emitting devices and transparent conducting electrodes [2]. Zinc oxide (ZnO) is a II–VI n-type semiconductor with a wide band gap, large free exciton binding energy (60 meV), high transparency in the visible region and a wide range resistivity values (10^{-4} to 10^{12} Ω cm) [3]. Due to their optical and electrical properties metal oxide semiconductor films have been widely studied and received considerable attention in recent years. Some of them are good candidates for the application in transparent conductive films, if they are prepared off-stoichiometry or doped with suitable impurities. ZnO is one of the metal oxide semiconductors suitable for use in optoelectronics and an alternative material to ITO [4]. The electrical conductivity of zinc oxide depends on the carrier concentration contributed by oxygen vacancies or interstitial metal atoms in it [5]. Molybdenum (Mo) is one of the potential dopant materials for improving conductivity and transparency of the zinc oxide thin films. The substitution of Mo is possible due to the smaller radius of Mo (0.062 nm) compared to Zn (0.083 nm). Moreover, Mo ([Kr]: $4d^5 5s^1$) is the more beneficial impurity to be doped into the ZnO matrix as it can donate 4 electrons to the free carriers due to the high valence difference between Mo^{6+} ions and substituted Zn^{2+} ions. Therefore, very small amount of

* Corresponding author. Tel.: +91 431 2503611; fax: +91 431 2500133.
E-mail addresses: swapna.ramella@yahoo.com (R. Swapna), santhoshmc@nitt.edu, santhoshmc@yahoo.com (M.C. Santhosh Kumar).

0272-8842/$36.00
doi:10.1016/j.ceramint.2012.01.039

Mo doping can give enough free carriers and reduce the ion scattering effect [6]. The investigations on MZO films are valuable in exploring substitute materials for ITO and may have potential application prospects in transparent optoelectronic devices.

Different deposition techniques are used to prepare MZO thin films such as RF/DC sputtering [7,8] and ion beam sputtering deposition (IBSD) [9]. In comparison to other chemical deposition techniques, spray pyrolysis [10] has several advantages such as high purity and excellent control of chemical uniformity in multi-component system. Spray pyrolysis has been developed as a powerful tool to prepare various kinds of thin films such as metal oxides and nanophase materials. Another advantage of the spray pyrolysis technique is that it can be adapted easily for production of large-area films. Investigations on the preparation and characterization of MZO films are less in the literature. Xiu et al. [7] used RF magnetron sputtering to deposit MZO films onto a glass substrate was one of such reports. In the present study, transparent and conductive Mo doped ZnO thin films (MZO) are prepared at different substrate temperatures (T_s) using a spray pyrolysis method and the effect of substrate temperature (T_s) on the structural, optical, electrical and photoluminescence properties of MZO films was investigated.

2. Experimental

Mo doped ZnO thin films were prepared by spray pyrolysis technique at substrate temperatures of 573 K, 623 K, 673 K and 723 K. The precursor solution for spray pyrolysis was prepared by dissolving an appropriate amount of zinc acetate dehydrate (Sigma–Aldrich, 99.5%, Germany) and molybdenum chloride (Sigma–Aldrich, 99%, USA) in the 100 ml mixture of deionized water and ethanol (Merck, 99.9%, Germany) at room temperature. A small amount of acetic acid (Merck, 99.9%, Germany) was added into the solution to avoid forming milky precipitate of hydroxides [11]. The concentration of Mo was 2 at.% and total concentration of the solution was maintained at 0.1 M. The glass substrates were cleaned with detergent solution and deionized water. Ultrasonic cleaning was carried out for 30 min in an ultrasonic bath and then rinsed in acetone for 10 min. The film deposition was carried out in Holmarc (India) spray pyrolysis unit. The spray nozzle was at a distance of 20 cm from the substrate during deposition and solution flow rate was held constant at 3 ml/min. Air was used as the carrier gas, at the pressure of 2 bar. When aerosol droplets come close to the substrates, a pyrolytic decomposition process occurs and high quality MZO films were produced.

The structural properties were studied by X-ray diffraction (XRD) measurements using Rigaku D/Max ULTIMA III diffractometer with CuK_α radiation ($\lambda = 1.5406$ Å). The thickness was measured using Stylus profile meter. The surface morphology was studied by a scanning electron microscope (S3000N, Hitachi). Atomic force microscopy (NTMDT-NTEGRA, Russia) was used to analyze the surface morphology and roughness of the films. The optical measurements of Mo doped ZnO thin films were carried out at room temperature using Shimadzu UV-1700 Spectrophotometer in the wavelength range 300–1100 nm. Photoluminescence spectra were recorded at room temperature using Perkin Elmer LS 55 Luminescence spectrometer with an excitation wavelength of 325 nm. Electrical resistivity, carrier concentration and mobility were measured at room temperature on a Hall system (Ecopia, Model: HMS-5000) using the van der Pauw method.

3. Results and discussions

3.1. Structural studies

Fig. 1 shows the XRD patterns of 2 at.% MZO thin films deposited by spray pyrolysis at different substrate temperatures. Spray pyrolysis is a chemical deposition technique where the endothermic thermal decomposition takes place at the hot surface of the substrate to give the final product. The substrate temperature plays an important role in the film formation. When the substrate temperature is below 553 K, the spray falling on the substrate undergoes incomplete thermal decomposition (oxidation) giving rise to a foggy film whose transparency as well as electrical conductivity is very poor. If the substrate temperature is too high (>773 K), the spray gets vaporized before reaching the substrate and the film becomes almost powdery. Whereas at optimum substrate temperature in the range of 573–723 K, the spray reaches the substrate surface in the semi-vapor state and complete oxidation will take place to give clear MZO film as a final product [12].

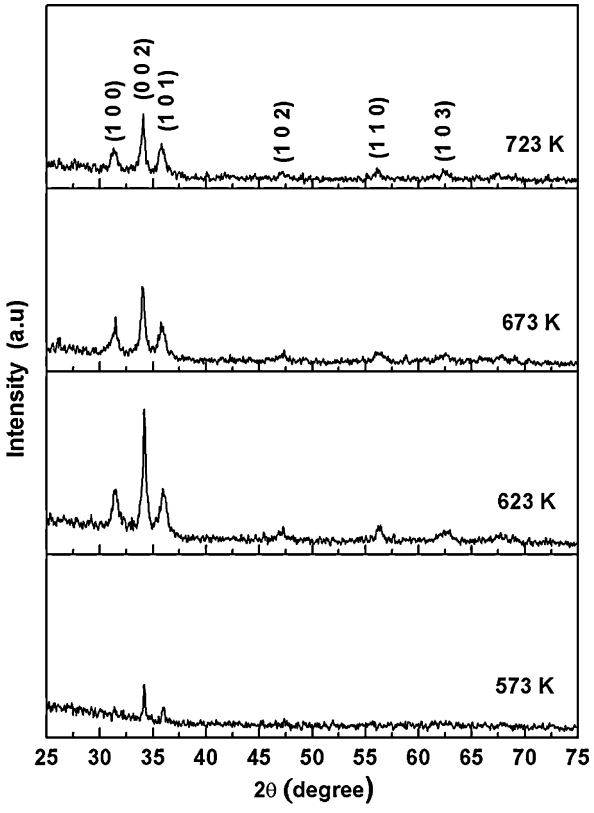

Fig. 1. X-ray diffraction patterns of the MZO films with different substrate temperatures.

Table 1
Calculated TC, lattice constants, thickness, strain, stress and optical band gap values of MZO films with different substrate temperatures.

Substrate temperature (K)	Thickness (nm)	TC of (0 0 2)	Lattice constants		Strain (%)	Stress (GPa)	Band gap E_g (eV)
			a (Å)	c (Å)			
573	1515	1.65	3.268	5.252	1.11	−5.06	3.270
623	1400	2.21	3.265	5.250	1.08	−4.93	3.256
673	1180	2.03	3.267	5.253	1.13	−5.15	3.241
723	984	1.94	3.272	5.259	1.25	−5.67	3.233

The XRD measurements reveal that all the films are polycrystalline with a wurtzite structure and a preferred orientation with the c-axis perpendicular to the substrates. Six well-defined peaks, identified as the (1 0 0), (0 0 2), (1 0 1), (1 0 2), (1 1 0) and (1 0 3) diffraction planes of ZnO. No peaks corresponding to either molybdenum, zinc or any of its oxides were observed in the XRD patterns, which indicate that there is no additional phase present in Mo-doped ZnO films. Films grown at 623 K shows strong preferred orientation with c-axis perpendicular to the substrate. The peak intensity is found to be high for the samples prepared at 623 K indicating a better crystallinity. So, 623 K is the optimum temperature to obtain uniform well adherent MZO films. For the films deposited at 573 K, the XRD peak intensity is low because of the low crystalline growth of the films on substrate surface due to insufficient thermal energy. From Table 1, it is seen that film thickness decreases with increase in deposition temperature. The decrease in film thickness with deposition temperature may be attributed to the increase in evaporation rate of the initial product with increase in substrate temperature [12]. The intensity of the peak shows a significant decrease as the substrate temperature increases from 623 to 723 K. This indicates the deterioration of crystallinity and strain is induced at high substrate temperatures. The average crystallite sizes of the films deposited at different substrate temperatures have been calculated using Scherrer's formula [13]:

$$D = \frac{k\lambda}{\beta\cos\theta} \tag{1}$$

where λ is the wavelength of CuK_α radiation (1.5406 Å), k is shape factor (0.9), β is the broadening of the diffraction line (FWHM) and θ is Bragg's diffraction angle. The instrumental broadening effect has been subtracted from the FWHM using the XRD pattern of a standard silicon sample. The full width at half maximum (FWHM) and crystallite size as a function of film substrate temperature is shown in Fig. 2. The FWHM of the peak decreases up to a substrate temperature of 623 K, thereafter it increases with the increase in substrate temperature. The average crystallite size of the films increases from 17 nm to 28 nm with the increase of substrate temperature from 573 K to 623 K, thereafter it slightly decreases with further increase of substrate temperature to 723 K. The temperature dependence of crystallinity may be interpreted as follows. When substrate temperature increases, the oxygen deficiency leads to the growth of less homogeneous films with more crystallographic faults. It suggests that the non-stoichiometric films show poor crystallinity [7].

The preferential or random growth of polycrystalline thin films can be understood by calculating the texture coefficient TC ($h\,k\,l$) for all planes. The texture coefficient is calculated using the following equation [14]:

$$TC(h\,k\,l) = \left(\frac{I_{(h\,k\,l)}/I_{o(h\,k\,l)}}{\frac{1}{N}\sum I_{(h\,k\,l)}/I_{o(h\,k\,l)}}\right) \tag{2}$$

where $I_{(h\ k\ l)}$ indicate the X-ray diffraction intensities obtained from the films, and N is the number of reflections observed in the XRD pattern. $I_{o(h\ k\ l)}$ is the intensity of the standard diffraction pattern (JCPDS card 75-0576). It is clear from the definition that the deviation of texture coefficient from unity implies the film growth occurs in certain preferred orientation. Table 1 shows the variation of the texture coefficient with variation of substrate temperatures for the (0 0 2) plane. The higher value of texture coefficient at 623 K indicates the preferred orientation of the film along that diffraction plane (0 0 2). However, the intensity of (0 0 2) diffraction peak had a tendency to decrease with an increase in substrate temperature. This presumably is due to the strain occurring in the MZO thin films. The lattice constants 'a' and 'c' were calculated using the following equation [15]:

$$\frac{1}{d_{hkl}^2} = \frac{4}{3}\left[\frac{h^2+hk+k^2}{a^2}\right] + \frac{l^2}{c^2} \tag{3}$$

The lattice constants 'a' and 'c' values are found to be larger than that of bulk ZnO values of 0.3242 nm and 0.5194 nm (JCPDS-75-0576) as shown in Table 1. It may be due to Mo^{6+}

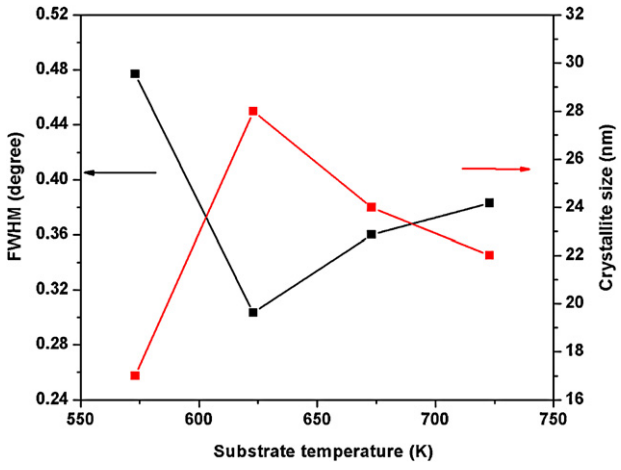

Fig. 2. Variation of FWHM and crystallite size as a function of substrate temperature.

ions substituted Zn^{2+} ions in the ZnO matrix as significantly affecting the lattice parameter. Because, the ionic radius of Mo^{6+} (0.62 Å) smaller than that of Zn^{2+} (0.83 Å). The strain ε_z in the lattice along the *c*-axis has been estimated from the lattice parameters using the following expression [16]:

$$\varepsilon_Z = \frac{c_{film} - c_{bulk}}{c_{bulk}} \times 100\% \quad (4)$$

where 'c_{film}' is the *c*-axis lattice constant calculated from the XRD peak position and 'c_{bulk}' is the *c*-axis lattice constant of bulk ZnO. In thin films, strain originates mainly due to a mismatch between the polycrystalline film and the amorphous substrate and/or differences in coefficients of thermal expansion of the film and the substrate. The strain in the films is likely to be of intrinsic, rather than of thermal origin. The thermal strain introduced by the different linear thermal expansion coefficients α of film ($\alpha_{ZnO} = 4 \times 10^{-6}\,K^{-1}$) and glass substrate ($\alpha_{glass} = 9 \times 10^{-6}\,K^{-1}$) is significantly smaller than the measured strain. The lattice constant '*c*' of MZO films is larger than the bulk ZnO. This indicates that the films have residual tensile strain along the *c*-axis. We have calculated the stress in the plane of the films based on the biaxial strain model [17], using the following formula.

$$\sigma_{film} = \frac{2C_{13}^2 - C_{33}(C_{11} - C_{12})}{C_{13}} \times \varepsilon_Z \quad (5)$$

where $C_{11} = 209.7$ GPa, $C_{12} = 121.1$ GPa, $C_{13} = 105.1$ GPa and $C_{33} = 210.9$ GPa are the elastic stiffness constants of bulk ZnO. According to the above equation, if the stress is positive, the biaxial stress is tensile and if the stress is negative, the biaxial stress is compressive. The compressive stress and strain are as shown in Table 1. The total stress in the film commonly consists of two components. One is the intrinsic stress introduced by impurities, defects and lattice distortions in the crystal, and the other is the extrinsic stress introduced by the lattice mismatch and thermal expansion coefficient mismatch between the film and substrate. In the present case, the extrinsic stress will not be present and the total estimated stress values seem to be dominantly intrinsic. The MZO films deposited at higher temperature exhibit strong compressive stress. Whereas the samples prepared at 623 K show a small decrease in stress, this may be attributed to the variation in crystallite size or morphology of the film. The stress increases slightly at the temperature of 723 K indicative of possible effect of lattice distortions and defects [16].

3.2. Morphological studies

The substrate temperature dependence of crystallinity and crystallite sizes for the MZO films were further revealed by their SEM micrographs. Fig. 3(a), (b), (c) and (d) shows the SEM morphologies of MZO films deposited at 573 K, 623 K, 673 K and 723 K, respectively. The microstructure of the films consists of many spherical grains distributed uniformly

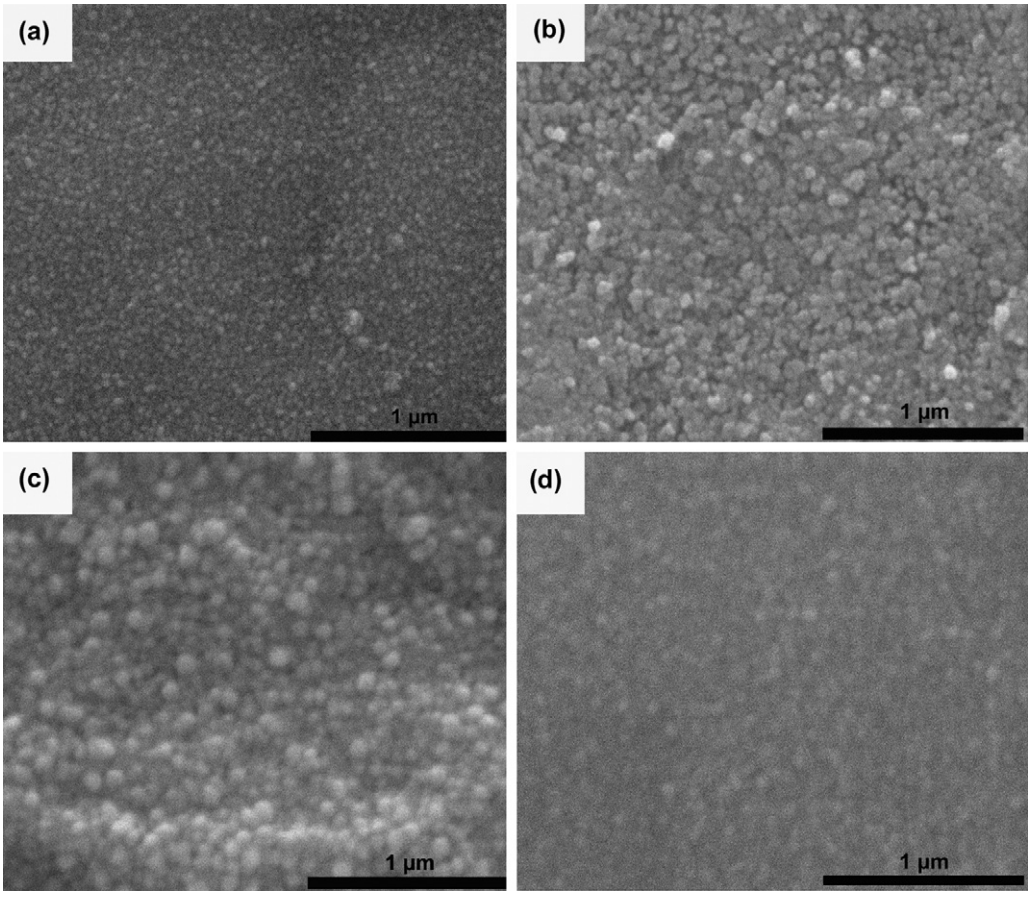

Fig. 3. SEM images of the MZO films with various substrate temperatures (a) 573 K (b) 623 K (c) 673 K and (d) 723 K.

throughout the surface. The surface morphology of the MZO thin films deposited at low substrate temperature (573 K) show small but dense grains. When the substrate temperature increases to 623 K, the number of nuclei increases and the nuclei grow over the whole surface area of the substrate with uniform grains. The grain size became smaller with increase of substrate temperature to 723 K. This is mainly due to the migration ability of atoms and molecules on the surface are increased during the growth at higher substrate temperature. This is an evidence for increase of the film stress with the increase in substrate temperature. It can be seen that with increase in substrate temperature, the grain size of the films also found to detoriets. This is consistent with the results of XRD studies.

Fig. 4(a) and (b) shows AFM Images 2D and 3D of MZO thin films deposited under different substrate temperatures. The scanning area was 2 μm × 2 μm. From the surface morphology of the films it is observed that the grain growth is of nanometer size with uniform structure. The particle size is found to decrease with increase in substrate temperature. But the particle size seems to appear larger for 723 K than for 673 K from the 3D-AFM image. At higher substrate temperature, re-evaporation competes with the formation of nuclei, resulting in fewer, but larger, nuclei. Growth of these larger nuclei is more three-dimensional than in films prepared at lower temperature. The coalescence should result in large and irregularly shaped grains [18]. To find film uniformity, we measured the surface rms (root mean square) and average roughness of MZO films. It is seen that the films deposited at various substrate temperatures show different surface roughness. At the substrate temperature of 673 K, the average and rms (root mean square) roughness are very low as 4.105 nm and 5.231 nm, respectively. The substrate temperature is further increased to 723 K, the values of average roughness and rms roughness increases to 11.874 nm and 14.940 nm. The initial reduction in the roughness with substrate temperature is attributed to island coalescence. The measured size of the particle from the AFM surface images is higher than the values calculated from XRD studies, indicating that these particles are probably an aggregation of small crystallites on the surface of the films.

3.3. Electrical studies

Fig. 5 shows the electrical resistivity (ρ), carrier concentration (n) and mobility (μ) as function of substrate temperature. Hall effect measurements shows that all the prepared films are n-type after Mo doping with different substrate temperatures. The films deposited at 573 K exhibit a resistivity of $7.28 \times 10^{-2}\ \Omega$ cm. As the substrate temperature increases to 623 K, the resistivity decreases to the minimum value of $6.22 \times 10^{-2}\ \Omega$ cm, which is due to the improved Mo substitution in ZnO (MZO) film crystallinity. Similar results were also obtained in Zr-doped In_2O_3 thin films [19]. At this temperature the Hall mobility also undergoes an increase, which results from the greatly weakened carrier scattering process due to the improvement of crystallinity. The increase of both carrier concentration and Hall mobility results in a reduction in resistivity. The maximum carrier concentration

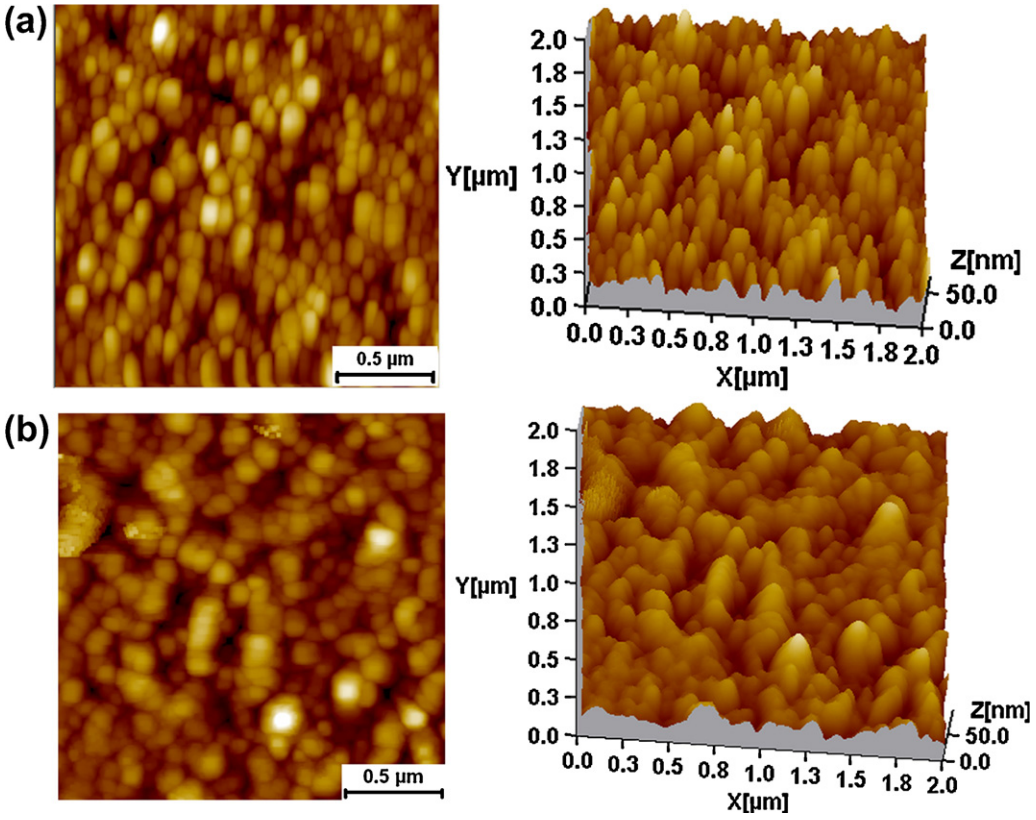

Fig. 4. AFM 2D and 3D images of the MZO films with: (a) substrate temperature 673 K and (b) substrate temperature 723 K.

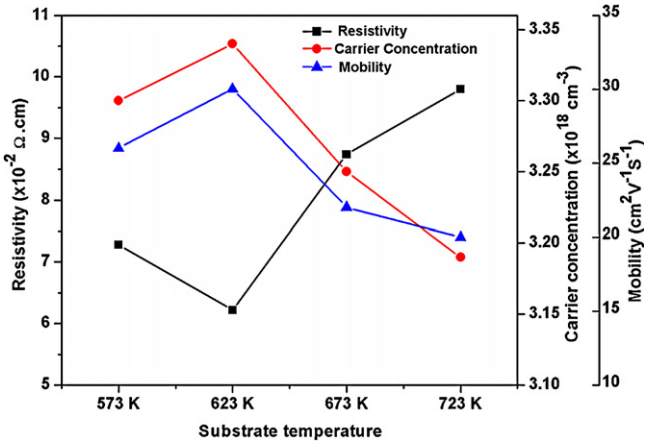

Fig. 5. Variation of electrical resistivity (ρ) carrier concentration (n) and mobility (μ) of the MZO films with substrate temperature.

and Hall mobility are 3.34×10^{18} cm^{-3} and 30 cm^2/VS, respectively, which are obtained for samples deposited at the substrate temperature of 623 K. A further increase in substrate temperature causes slight degradation of the electrical properties. The increase of the film resistivity is ascribed to both the reduction in the carrier concentration and carrier mobility. The increase of electrical resistivity should be attributed to the increase of the grain boundary scattering. As seen in Fig. 2, the crystallite size decreases with increasing substrate temperature. Smaller crystallite size results in a higher density of grain boundaries, which behaves as barriers for carrier transport and traps for free carrier. Hence, a decrease of crystallite size can cause an increase of grain boundary scattering [20]. The decrease of carrier concentration may be due to the decrease of native donors resulted from the enhancement of oxidation on the substrate surface [21]. Besides, the decrease of carrier concentration is also attributed to an increase in chemisorbed oxygen which acts as electron trap [22].

3.4. Optical studies

Fig. 6(a) shows the transmittance and Fig. 6(b) shows the reflectance spectra of the MZO films measured in the range of 300–1100 nm. The films formed at substrate temperature of 623 K showed 75% maximum transmittance, while the films formed at higher substrate temperature (723 K) exhibit the lowest optical transmittance of 58% in the visible region. It is seen that the transmittance is limited only by the surface reflectance of about 8.5%. The decrease of transmittance at higher substrate temperature may be attributed to the increased scattering of photons by rough surface morphology and crystal defects. It may also be due to conversion of crystalline MZO films to non-crystalline with the increase of substrate temperature. All samples show sharp absorption edge near to 375 nm in the UV region and these absorption edges slightly shift to longer wavelengths. The absorption coefficient is calculated from the relation [23]:

$$T = (1 - R)\exp(-\alpha t) \tag{6}$$

where T is the transmittance, R is the reflectance, and t is the film thickness. The optical band gap of the films is determined from transmittance spectra by applying the Tauc model [24]:

$$\alpha h\nu = B(h\nu - E_g)^n \tag{7}$$

where E_g is the optical band gap, $h\nu$ is the incident photon energy and B is the constant and n can have values 1/2, 3/2, 2 and 3 depending up on the mode of inter band transition, i.e. direct allowed, direct forbidden, indirect allowed and indirect forbidden transition respectively. For n = 1/2 the transition data provide the best linear curve in the band edge region, implying the transition is direct in nature. The band gaps of the films have been calculated using Tauc's plot by plotting $(\alpha h\nu)^2$ versus $h\nu$ as shown in Fig. 7 and by extrapolating the linear portion of the absorption edge to find the intercept with energy axis. The inset of Fig. 7 depicts the change in optical band gap as a function of substrate temperature. In the present study, the film substrate temperature increases from 573 K to 723 K, the value of the optical band gap gradually decreases from 3.270 to 3.233 eV. The optical band gap of the MZO films decreases with increase in carrier concentration from 573 K to 623 K, thereafter carrier concentration slightly decrease with further increase of substrate temperature to 723 K. Generally, defects are accumulated at the grain boundaries. Smaller grain size results in a tensile

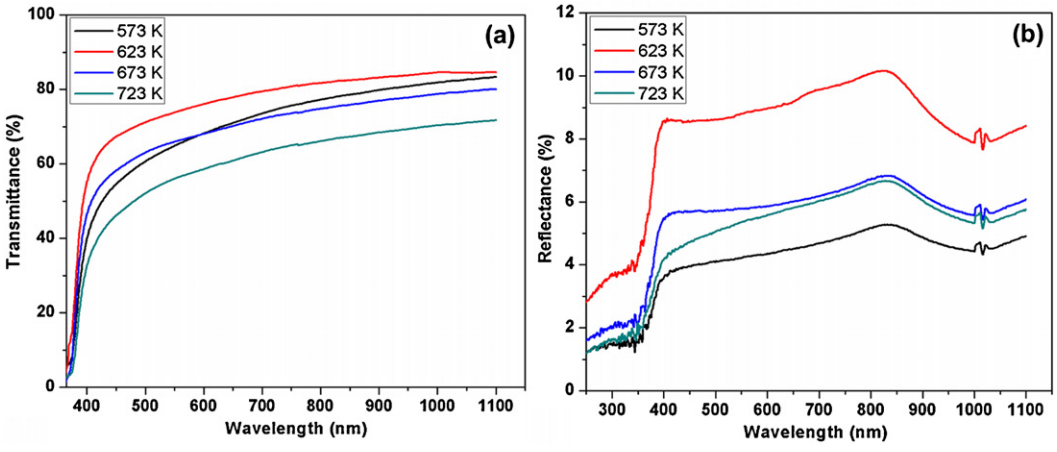

Fig. 6. (a) Transmittance and (b) reflectance spectra of MZO films for different substrate temperatures.

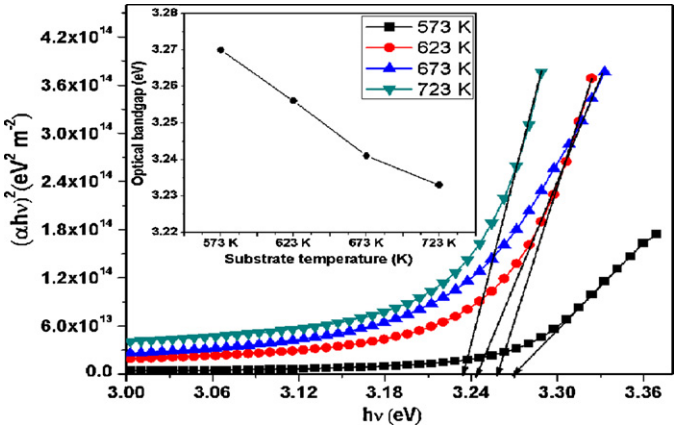

Fig. 7. Variation of $(\alpha h\nu)^2$ vs. $h\nu$ of the MZO thin films.

strain arising from thermal mismatch between the MZO film and the substrate. This indicates that the presence of large number of grain boundaries increases the defects in the film. The defects could act as the radiative recombination centers that emit visible light, which causes transition to lower band observed as shrinkage in band gap [25]. However, our optical band gap results indicate that the Burstein–Moss effect is weak. According to Brustein–Moss effect, raising the Fermi level into the conduction band of a degenerate semiconductor leads to energy band broadening [26]. Therefore the shrinkage effect is dominant over the Burstein–Moss effect, since the E_g values decreases with the increase of substrate temperature.

The complex refractive index and dielectric function characterize the optical properties of any solid material. The refractive index of the film was calculated by the following relation [27]:

$$R = \frac{(n-1)+k^2}{(n+1)+k^2} \tag{8}$$

where k ($k = \alpha\lambda/4\pi$) is the extinction coefficient. The refractive index (n) and extinction coefficient (k) with the function of wavelength is shown in Fig. 8. The refractive index values of

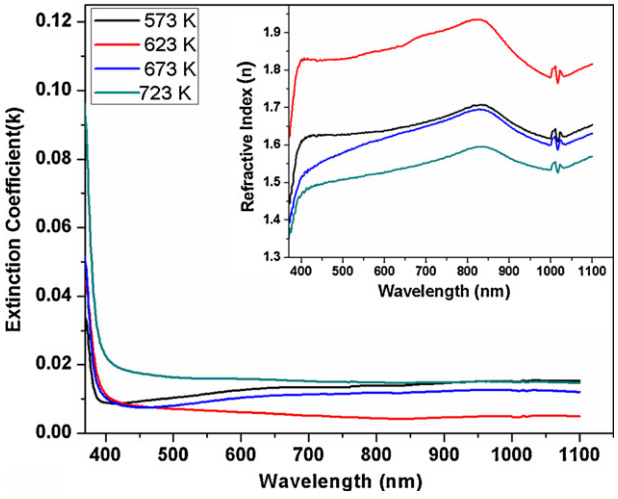

Fig. 8. The variation of refractive index and extinction coefficient of the MZO films with various substrate temperatures.

the MZO film increase up to certain value of wavelength and then decrease. The calculated values in the visible region are in agreement with the values reported in the literature [28]. The extinction coefficient (k) of the MZO film decreases with the increasing of wavelength in the visible region and then attains almost constant value toward higher wavelengths, while it increases in the ultraviolet region. The fundamental electron excitation spectrum of the film is described by means of a frequency dependence of the complex electronic dielectric constant. The dielectric constant is defined as $\varepsilon(\omega) = \varepsilon_1(\omega) + i\varepsilon_2(\omega)$, the real and imaginary parts of the dielectric constant are related to the n and k values. The ε_1 and ε_2 values are calculated using the formulae [29]:

$$\varepsilon_1(\omega) = n^2(\omega) - k^2(\omega) \tag{9}$$

$$\varepsilon_2(\omega) = 2n(\omega)k(\omega) \tag{10}$$

The variation of the real (ε_1) and imaginary (ε_2) parts of the dielectric constant for different substrate temperatures is illustrated in Fig. 9(a) and (b). The figures revealed that the values of the real part are higher than that of the imaginary part. It can be seen that the imaginary part of the dielectric constant decreases sharply with the increasing of wavelength from UV region to visible region. In the visible region, it then attains almost a constant value.

3.5. Photoluminescence studies

Room temperature PL emission spectra for all the samples are measured in the wavelength range of 350–600 nm at an excitation wavelength of 325 nm. PL spectra of MZO films with different substrate temperatures are shown in Fig. 10. The ZnO emission is generally classified into two categories. One is the UV emission of the near band edge in the UV region related to free-exciton recombination and other is the deep-level (DL) emission in the visible range. Biaxial strain in ZnO films affects only UV emission and causes no change in the position or intensity of deep level emission. The photoluminescence spectra show a violet emission band around 400–430 nm, but no UV emissions are observed in Mo-doped ZnO thin films. The violet peak at 425 nm (2.92 eV) can be attributed to the Zn vacancies [30,31]. Prabakar et al. [32] reported a violet emission band (centered at 420 nm) attributed to radiation transition related interface traps existing at the grains boundaries. Jin et al. [31] observed violet emission centered at 420 nm for ZnO films deposited by pulsed laser deposition (PLD). They observed that the violet emission was due to a defect level in the grain boundaries of the ZnO crystals. Zhang et al. [33] reported a green emission at a wavelength of 490 nm. In present case, the peak at 486 nm (2.55 eV) is green emission, which originates from the defect emission of oxygen vacancies [34]. The PL spectrum of the undoped ZnO film shows a very broad feature at 530 nm due to the presence of interstitial oxygen defects in ZnO films [35]. However, the broad feature at 530 nm (2.34 eV) appears as green emission in the case of Mo-doped ZnO films. It is well known that such broad deep level emission is closely related to intrinsic defects such as Zn_i and

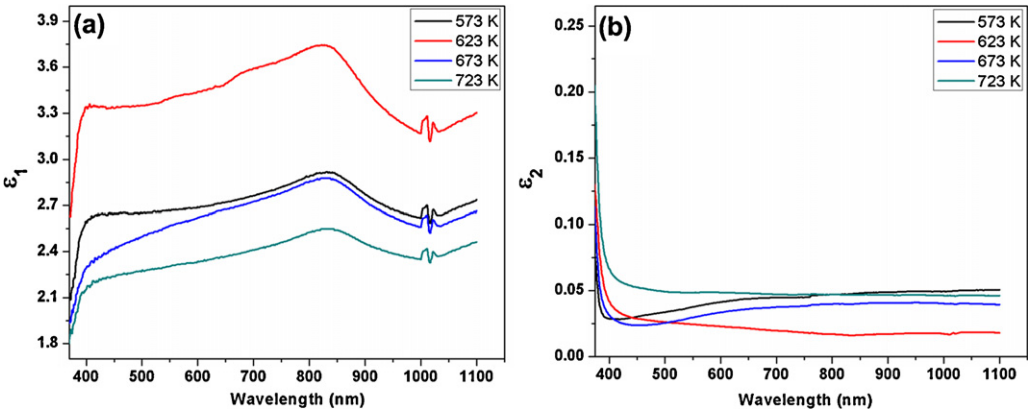

Fig. 9. The variation of (a) real part and (b) imaginary part of dielectric constant of the MZO films with wavelength.

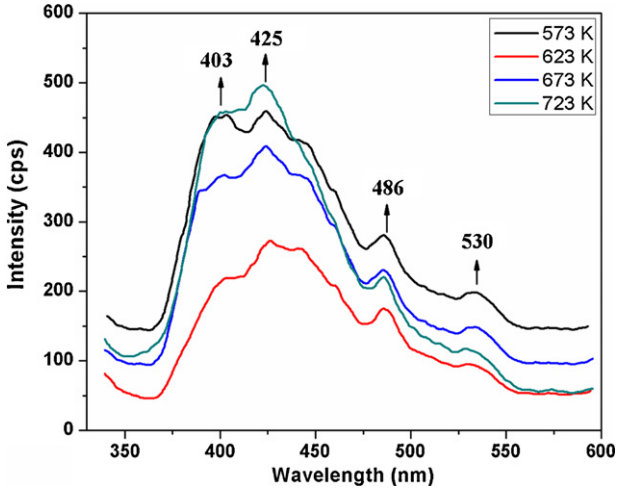

Fig. 10. Photoluminescence spectra of MZO films with various substrate temperatures.

V_O [36]. Generally, the luminescence property of the films has a close relation with the film crystallinity because the density of defects in film reduces with an improvement of the crystallinity [16].

4. Conclusions

In this study, the influence of the substrate temperature on the structural, surface morphology, optical and electrical properties of MZO thin films grown on glass substrates by spray pyrolysis was investigated. From the X-ray diffraction (XRD) pattern, it was observed that the MZO thin films were polycrystalline with wurtzite structure. From AFM studies, it was found that the surface roughness of the thin films increases with the increase of substrate temperature. SEM analysis revealed the surface morphology of the films is uniform and morphology of the film varying with the substrate temperature. The optical band gap of 3.256 eV was observed for the films formed at 623 K. The lowest resistivity achieved is $6.22 \times 10^{-2}\,\Omega\,\text{cm}$ with a high mobility of $30\,\text{cm}^2/\text{VS}$ for the films deposited at 623 K. The photoluminescence (PL) spectra observed that all the thin films produced violet and green emissions in the visible region.

Acknowledgement

Author M. C. S. Kumar is thankful to the Department of Science and Technology (DST), Govt. of India for the financial support through SERC-Fast Track project for young Scientists.

References

[1] Z. Deheng, Z. Dejun, W. Qingpu, Effect of substrate temperature on properties for transparent conducting ZnO:Al films on organic substrate deposited by r.f sputtering, J. Mater. Sci. Technol. 17 (5) (2001) 517–520.
[2] Ü. Özgür, Y.I. Alivov, C. Liu, A. Teke, M.A. Reshchikov, S. Doğan, V. Avrutin, S.-J. Cho, H. Morkoç, A comprehensive review of ZnO materials and devices, J. Appl. Phys. 98 (2005) 041301–141301.
[3] Y.T. Chien, S.F. Kai, W.W. Yu, J.C. Chi, K.T. Yung, K.L. Chung, Transparent semiconductor zinc oxide thin films deposited on glass substrates by sol–gel process, Ceram. Int. 36 (2010) 1791–1795.
[4] B.Y. Oh, M.C. Jeong, W. Lee, J.M. Myoung, Properties of transparent conductive ZnO:Al films prepared by co-sputtering, J. Cryst. Growth 274 (2005) 453–457.
[5] D.S. Ginley, C. Bright, Transparent conducting oxides, MRS Bull. 25 (8) (2000) 15–21.
[6] H.K. Kim, S.H. Huh, J.W. Park, J.W. Jeong, G.H. Lee, The cluster size dependence of thermal stabilities of both molybdenum and tungsten nanoclusters, Chem. Phys. Lett. 354 (2002) 165–172.
[7] X. Xiu, Y. Cao, Z.Y. Pang, S. Han, Effects of substrate temperature on the properties of Mo-doped ZnO films prepared by RF magnetron sputtering, J. Mater. Sci. Technol. 25 (6) (2009) 785–788.
[8] J.L. Shi, H. Ma, G.H. Ma, H.G. Ma, J. Shen, Structure and ultrafast carrier dynamics in n-type transparent Mo:ZnO nanocrystalline thin films, Appl. Phys. A 92 (2008) 357–360.
[9] C.C. Kuo, C.C. Liu, S.C. He, J.T. Chang, J.L. He, Influence of assistant ion beam on the opto-electrical properties of molybdenum doped zinc oxide films deposited on polyethersulfone via dual ion beam sputtering, Vacuum 85 (2011) 961–967.
[10] D.J. Seo, S.H. Park, Structural, electrical and optical properties of In_2O_3:Mo films deposited by spray pyrolysis, Physica B 357 (2005) 420–427.
[11] C.M. Muiva, T.S. Sathiaraj, K. Maabong, Effect of doping concentration on the properties of aluminium doped zinc oxide thin films prepared by spray pyrolysis for transparent electrode applications, Ceram. Int. 37 (2011) 555–560.
[12] B.J. Lokhande, M.D. Uplane, Effect of deposition temperature on spray deposited cadmium oxide films, Mater. Res. Bull. 36 (2001) 439–447.

[13] K. Venkateswarlu, A. Chandra Bose, N. Rameshbabu, X-ray peak broadening studies of nanocrystalline hydroxyapatite by Williamson–Hall analysis, Physica B 405 (2010) 4256–4261.
[14] R. Romero, D. Leinen, E.A. Dalchiele, J.R. Ramos Barrado, F. Martin, The effects of zinc acetate and zinc chloride precursors on the preferred crystalline orientation of ZnO and Al-doped ZnO thin films obtained by spray pyrolysis, Thin Solid Films 515 (2006) 1942–1949.
[15] S. Suwanboon, P. Amornpitoksuk, A. Sukolrat, Dependence of optical properties on doping metal, crystallite size and defect concentration of M-doped ZnO nanopowders (M = Al, Mg, Ti), Ceram. Int. 37 (2011) 1359–1365.
[16] X.Y. Li, H.J. Li, Z.J. Wang, H. Xia, Z.Y. Xiong, J.X. Wang, B.C. Yang, Effect of substrate temperature on the structural and optical properties of ZnO and Al-doped ZnO thin films prepared by dc magnetron sputtering, Opt. Commun. 282 (2009) 247–252.
[17] M.K. Puchert, P.Y. Timbrell, R.N. Lamb, Post deposition annealing of radio frequency magnetron sputtered ZnO films, J. Vac. Sci. Technol. A 14 (4) (1996) 2220–2230.
[18] A.V. Moholkar, G.L. Agawane, K.U. Sim, Y. bin Kwon, K.Y. Rajpure, J.H. Kim, Influence of deposition temperature on morphological, optical, electrical and opto-electrical properties of highly textured nano-crystalline spray deposited CdO:Ga thin films, Appl. Surf. Sci. 257 (2010) 93–101.
[19] H. Kim, J.S. Horwitz, G.P. Kushto, S.B. Qadri, Z.H. Kafafi, D.B. Chrisey, Transparent conducting Zr-doped In_2O_3 thin films for organic light-emitting diodes, Appl. Phys. Lett. 78 (2001) 1050–1052.
[20] H. Kim, J.S. Horwitz, G. Kushto, A. Pique, Z.H. Kafafi, C.M. Gilmore, D.B. Chrisey, Effect of film thickness on the properties of indium tin oxide thin films, J. Appl. Phys. 88 (2000) 6021–6025.
[21] X.Q. Gu, L.P. Zhu, Z.Z. Ye, Q.B. Ma, H.P. He, Y.Z. Zhang, B.H. Zhao, Highly transparent and conductive $Zn_{0.85}Mg_{0.15}O$:Al thin films prepared by pulsed laser deposition, Sol. Energy Mater. Sol. Cells 92 (2008) 343–347.
[22] Q.B. Ma, Z.Z. Ye, H.P. He, L.P. Zhu, W.C. Liu, Y.F. Yang, L. Gong, J.Y. Huang, Y.Z. Zhang, B.H. Zhao, Highly near-infrared reflecting and transparent conducting ZnO:Ga films: substrate temperature effect, J. Phys. D: Appl. Phys. 41 (2008) 055302–055306.
[23] T. Prasada Rao, M.C. Santhoshkumar, Highly oriented (1 0 0) ZnO thin films by spray pyrolysis, Appl. Surf. Sci. 255 (2009) 7212–7215.
[24] D. Jiles, Introduction to the Electronic Properties of Materials, Chapman and Hall, New York, 1994, p. 180.
[25] K.P. Bhuvana, J. Elanchezhiyan, N. Gopalakrishnan, T. Balasubramanian, Influence of grain size on the properties of AlN doped ZnO Mater, Sci. Semicond Process. 14 (2011) 84–88.
[26] Q.B. Ma, Z.Z. Ye, H.P. He, L.P. Zhu, J.Y. Huang, Y.Z. Zhang, B.H. Zhao, Influence of annealing temperature on the properties of transparent conductive and near-infrared reflective ZnO:Ga films, Scripta Mater. 58 (2008) 21–24.
[27] F. Abeles (Ed.), Optical Properties of Solids, North-Holland Publishing Company, London, UK, 1972.
[28] S.W. Xue, X.T. Zu, W.G. Zheng, H.X. Deng, X. Xiang, Effects of Al doping concentration on optical parameters of ZnO:Al thin films by sol–gel technique, Physica B 381 (2006) 209–213.
[29] J.N. Hodgson, Optical Absorption, Dispersion in Solids, Chapman and Hall, 1970.
[30] S.H. Jeong, B.S. Kim, B.T. Lee, Photoluminescence dependence of ZnO films grown on Si(1 0 0) by radio-frequency magnetron sputtering on the growth ambient, Appl. Phys. Lett. 82 (2003) 2625–2627.
[31] B.J. Jin, S. Im, S.Y. Lee, Violet and UV luminescence emitted from ZnO thin films grown on sapphire by pulsed laser deposition, Thin Solid Films 366 (2000) 107–110.
[32] K. Prabakar, C. Kim, C. Lee, UV, violet and blue-green luminescence from RF sputter deposited ZnO:Al thin films, Cryst. Res. Technol. 40 (2005) 1150–1154.
[33] D.H. Zhang, Z.Y. Xue, Q.P. Wang, J. Ma, Violet and blue photoluminescence emitted from ZnO films deposited by r. f. magnetron sputtering, Proc. SPIE 4918 (2002) 425–428.
[34] E. Kaminska, A. Piotrowska, J. Kossut, R. Butkute, W. Dobrowolski, R. Lukasiewicz, A. Barcz, R. Jakieła, E. Dynowska, E. Prze zdziecka, M. Aleszkiewicz, P. Wojnar, E. Kowalczyk, p-Type conducting ZnO: fabrication and characterisation, Phys. Status Solidi C 2 (2005) 1119–1124.
[35] Y. Liu, J. Lian, Optical and electrical properties of aluminum-doped ZnO thin films grown by pulsed laser deposition, Appl. Surf. Sci. 253 (2007) 3727–3730.
[36] B. Lin, Z. Fu, Y. Jia, Green luminescent center in undoped zinc oxide films deposited on silicon substrates, Appl. Phys. Lett. 79 (2001) 943–945.